Supplementary Information for

Photoprotection in Chlamydomonas: pH dependence, kinetics and light harvesting regulation

Lijin Tian*, Wojciech J. Nawrocki, Xin Liu, Iryna Polukhina, Ivo H.M. van Stokkum and Roberta Croce*

Biophysics of Photosynthesis, Department of Physics and Astronomy, Faculty of Science, Vrije Universiteit Amsterdam and Laser Lab Amsterdam. De Boelelaan1081, 1081 HV, Amsterdam, The Netherlands

*to whom the correspondence should be addressed. E-mail: l2.tian@vu.nl; r.croce@vu.nl

This file includes: Supplementary text 1-4.
Figs S1-S22
Table S1

Supplementary text 1

Isolation of thylakoid membrane and immunoblot analysis

The *C.reinhardtii* strain *cc124* was used as the WT strain. It was grown photoautotrophically in HSM under either low light (~20 μmol photons·m^{-2} s^{-1}) before any stress treatments or constant high light (~500 μmol photons·m^{-2} s^{-1}), - referred to as *cc124*-PHL. To stimulate the cells to express LHCSR1 and PsbS, the low light grown cells were exposed to two light conditions : 3-6 hours high light (~500 μmol photons·m^{-2} s^{-1}, *cc124*-3h/6h PHL) or 3~4 hours UV-B light (310 nm, 0.5 mW cm^{-2}, *cc124*-3h/4h UV-B). Both *stt7-9 (stt7-9* PHL*)* and the double mutant *npq4/stt7-9* (*npq4/stt7-9* PHL) were cultured under HL from time zero.

Thylakoid membranes from all strains were isolated as previously reported (1). Immunoblotting analysis was conducted as described in ref. (2).The pigments were extracted from the purified membranes by 80% acetone and the chlorophyll concentrations were estimated according to ref.(3). The same amount of chlorophylls were loaded on each well. The thylakoid membrane from Arabdopsis was employed as a positive control--.

When HL or UV-B light stress was applied to the culture, PsbS was detectable (Fig. S1*A*), whereas under continuous HL growth condition, a condition used in this work, PsbS did not accumulate in any of these three strains. Our immunoblot results are in good agreement with previous reports that PsbS is only transiently expressed in the cell and predominantly expressed under UV-B or short-period high light exposure (4-6).

Supplementary text 2

Global and sequential target analysis on 77 K time-resolved fluorescence data

To extract the ultrafast kinetics of light harvesting in *Chlamydomonas*, and to compare the two methods of NPQ induction, we fitted the streak camera images with a multi-exponential model in global analysis (see ref. (7) for the method and Fig. S6, S7 and Table S1 for the detailed explanation of all the Decay Associated spectra (DAS) components).

To double check if any new species (e.g.LHCII aggregates) emerges during NPQ, we performed a target analysis on the 77 K data, where the contribution of red emission originating from LHCII aggregation, if present, would be strongly enhanced (8). A sequential model (Fig. S12) was used to describe the excited state energy flow in the photosynthetic complexes. Four datasets were fitted simultaneously: UQ cells, acetic acid-induced Q cells (Q-AA), high-light induced Q cells (Q-HL) and isolated PSI. The last one was included in the fitting to provide spectral constraints for PSI. Note that the energy transfer rates within PSI were kept free to allow variations from the isolated system to the *in vivo* system, although they turned out to be similar (see Fig. S12). For cells in quenched conditions, we added extra energy relaxation pathways on all the PSII components, which is a reasonable approach for a sequential model without backward energy transfers. We found that this sequential model fits all four datasets satisfactorily, producing consistent spectra for PSII and PSI. Note that a fit in which we unlinked the spectra of the final energy trap in PSII, still results in very similar spectra for UQ and Q cells (Fig. S13). Therefore, we can conclude that no new species, like LHCII aggregates (which is expected to have a pronounced 700 nm peak), appear during the NPQ process. To highlight this fact, we have reconstructed the steady-state emission spectra of PSII in UQ and Q cells and compared them with the emission spectrum of LHCII aggregates in the membrane (Fig. S14). The fluorescence lifetime of the LHCII-aggregates is ~900 ps, and thus is heavily quenched compared to the 3.6 ns of the lifetime of trimeric LHCII (9) As shown in Fig. S14, the changes in spectral shape caused by aggregation are so substantial that they could not be missed in our fitting.

The fitted curves are plotted in Figs. S15-S18.

Supplementary text 3

Determination of the functional antenna size of PSII

Before the experiment, the algae were resuspended in high salt medium (HSM) (10) and dark-adapted for at least 30 minutes. Fluorescence induction curves were recorded at low light intensity (35 µmol photons m^{-2} s^{-1}, LED peak at 630 nm, roughly 20 e^- s^{-1} $PSII^{-1}$) in the presence of DCMU and upon addition of various concentrations of acetic acid.

To quantify the functional antenna size of PSII, the area delimited by the time zero of illumination, the maximal fluorescence level, and the induction curve was calculated for each experiment. This area corresponds to the average time of one electron transfer per PSII, assuming that the initial state is [P_{680}, Q_A] (open PSII RC) and the steady-state is [P_{680}, Q_A^-] (fully closed PSII). However, it is known that the addition of DCMU even to dark-adapted cells decreases the variable fluorescence due to an increase in the F_0 level (11), i.e. the initial fluorescence level in darkness ($F'_{0\ measured}$) does not represent the true F_0 value ($F'_{0\ actual}$). This occurs because of the presence of a $Q_B^{\cdot -}$ semiquinone in some PSII centers, which is in equilibrium with Q_A, and upon Q_B replacement with DCMU part of the Q_A remains in the reduced (Q_A^-) state (11). Moreover, after each illumination (and also due to the non-photochemical reduction of the PQ pool) in the presence of DCMU the quantity of open PSII RCs decreases due to the very slow oxidation of Q_A^- occurring on multiple timescales. It is thus crucial to compensate for the presence of closed centers in order to correctly calculate the areas above the fluorescence induction curves – and in consequence the functional antenna sizes - between samples with different fractions of open RCs. This correction is necessary to avoid confusion between the effect of NPQ, and the changes in PSII antenna size due to the closure of the centers since due to the connectivity between PSII RCs, some of the closed centers will increase the functional antenna size of a part of the remaining open RCs (12). One fact to clarify here is that despite the fluorescence rise curves always exhibit some sigmoidicity (11, 13), various biophysical models may be applied to describe them (14-16). Nonetheless, while our argument for F_0 correction is interpreted based on the "inter-unit excitation transfer model"(17) , it remains valid also for other models as long as the fluorescence rise is not mono-exponential (the latter being the only case where the derivative is directly proportional to the value of the function). We have done this in the absence of acid-induced NPQ by estimating $F_{0\ actual}$ through an extrapolation of the initial fluorescence kinetics to the value of F_0 measured in the absence of DCMU, in long-term dark-adapted algae (Fig. S21A, C). Although the fluorescence rise

presents some sigmoidicity, we have used a linear function to approximate the $F'_{0\ actual}$, as the error introduced by such approximation is one order of magnitude smaller than in the absence of the correction (compare Fig. S21B, D).

The situation is more complex in the quenched state. This is because one has no possibility to precisely measure the value of the light-quenched F_0 (F_0'), as the relaxation of NPQ and the oxidation of Q_A^- occur partially on the same timescale. Even with the acid-induced quenching the F_0' measurement is not optimal as acetate induces non-photochemical reduction of the PQ pool and as a consequence closes a fraction of the PSII RCs (18). We thus first assumed the same rate of NPQ in the presence- and absence of photochemical quenching (i.e. $k_{NPQ}=k_{NPQ\ Open}$), and calculated the F_0' value as $F_0'=F_0/[1+(F_0*NPQ/F_M)]$.

After the extrapolation, the F_0' and F_m' values were normalized to 0 and 1, respectively, to account for the single electron transfer between P_{680} and Q_A. In this way, the area above the fluorescence induction curve translates to the average time in which the open RC absorbs a photon and successfully produces a stable charge-separated state [P_{680},Q_A^-]. At a given low light intensity, a change in this area describes a change in the functional antenna size of PSII. The change in the functional antenna size was calculated as [(PSII_UQ - PSII_Q)/PSII_Q], which is the same way the NPQ is calculated, to facilitate the comparison between the two numbers. The value in the absence of acid is 0, and in case of the halving of the antenna size the value is 1. The NPQ value at each acid concentration was routinely calculated from the maximal fluorescence value at steady-state [(F_M - F_M'_acid)/F_M'_acid].

We then verified that the observed decrease of the functional antenna size upon quenching was not due to our calculations and the $k_{NPQ}=k_{NPQ\ Open}$ assumption (Fig. S22). We demonstrated this using two extreme cases : (i) by *not* compensating for the fraction of closed centers, as done by Belgio et al. (13), and by assuming $F_0'_{\ measured} = F_0'_{\ actual}$ (Fig. S22, blue squares) and (ii) by artificially overestimating the influence of NPQ by assuming that F_0' is quenched *to the same extent* as F_M', i.e. the F_v/F_M value being constant in the unquenched- and quenched state (Fig. S22, orange triangles). It is clear that for both of these incorrect assumptions, the trend of a decrease in functional antenna size upon NPQ is maintained - although to a different extent. We can then conclude that NPQ decreases the functional antenna size by competing with photochemistry.

We also note here that small variations in the value of F_0' (i.e. in the order of tens of % of the quenching rate, k_{NPQ}) do not initially have a strong influence on the total area above the fluorescenc curve. Given recent proposal that in flowering plants the $k_{NPQ\ Open}$ is 50% lower than the k_{NPQ} (19), we attempted to calculate the F_0' using this model. Upon low quenching, the antenna size decrease follows the data presented in the Fig. 4. However, in a case of strong quenching (NPQ > ~3), the value of the F_0' calulated using 50% lower k_{NPQ} in the open RCs becomes *higher* than the $F_{0\ measured}$, the latter already overestimated due to the reasons outlined above. Such result is inconceivable and proves that in *Chlamydomonas*, the $k_{NPQ\ Open}$ is the same, or very similar to the k_{NPQ}. This finally allowed us to validate the initial assumption used for the of F_0' calculation and led to conclude that in Chlamydomonas, the $k_{NPQ} \approx k_{NPQ\ Open}$.

Importantly, if one does not compensate for the closed centers (when $F_0'_{\ measured}$ is assumed to be equal to $F_0'_{\ actual}$), an apparent increase in functional antenna size in the presence of low NPQ will be observed (Fig. S21B). Furthermore, this increase would be larger if more RCs were closed upon fluorescence measurement. This is the case when DCMU is added to the thylakoids after a strong actinic light treatment which does not only activate NPQ, but also produces a large quantity of reductants that close a significant part of the RCs.

Supplementary text 4

LHCII:PSII Stoichiometry

The number of LHCII per PSII was estimated from the measured Chl *a/b* and PSI/PSII ratio as described in ref (20). The Chl *a/b* ratio was 2.46 and PSI/PSII ratio was 0.76 for the *stt7* mutant grown photoautotrophically in high light. According to our calculation (see details in ref.(20)), there are ~4.6 LHCII trimers per PSII resulting in nearly 200 Chls per PSII reaction center.

Figs. S1-S22

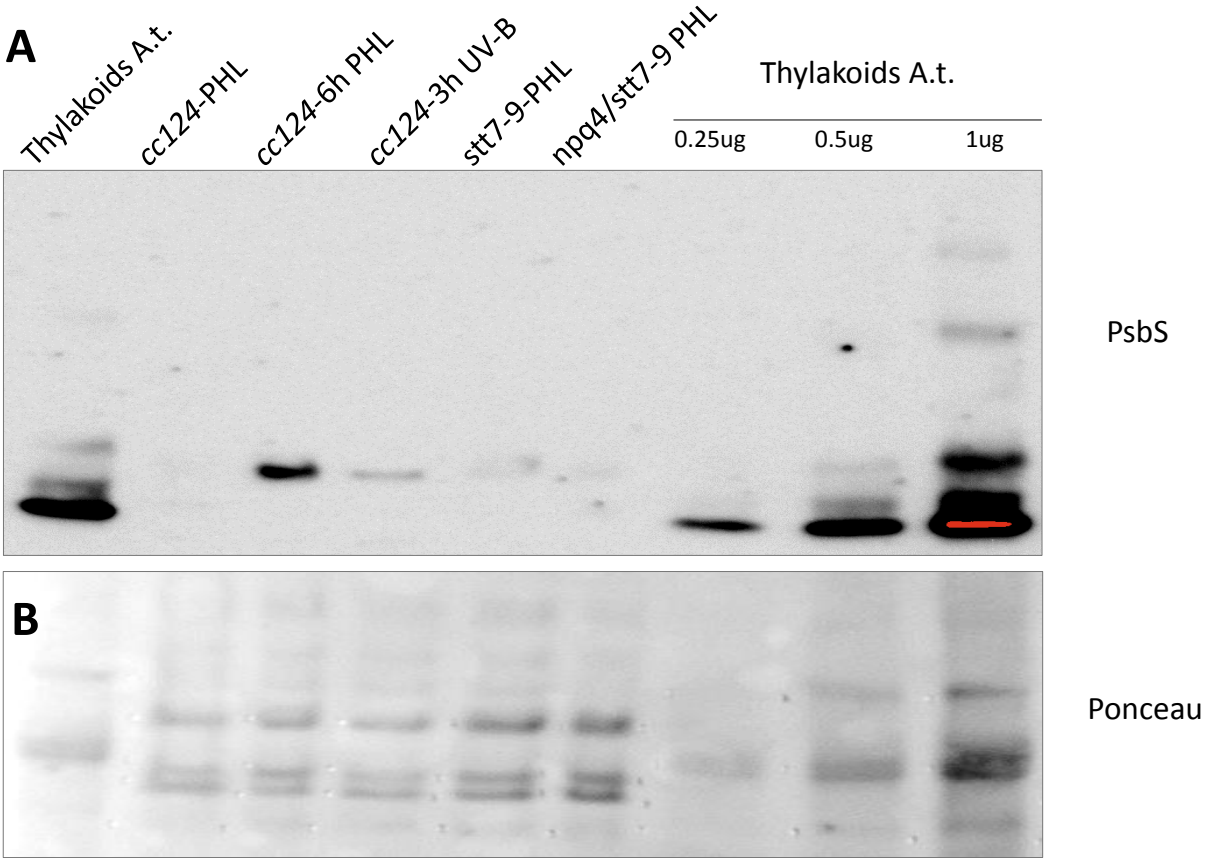

Fig. S1 Immunoblot results of PsbS (A) and the ponceau staining (B) in six samples , see detailed decription of the experiments and discussion in supplementary text 1. Please be aware that the bubbles seen in the ponceau are in between the membrane and the glass support for the picture and not on the membrane. All cells were cultured photoautotrophically in HSM.

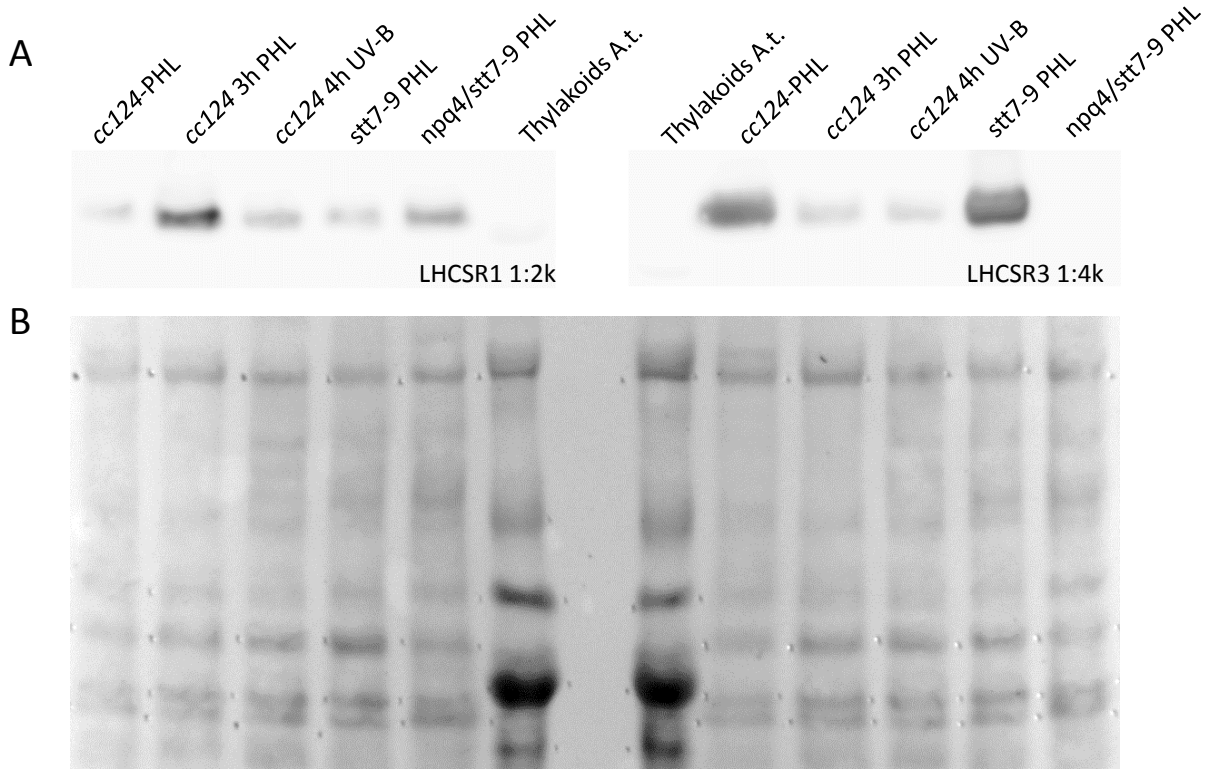

Fig. S2 Immunoblot results of LHCSRs (A) and the ponceau staining (B) in six samples , see detailed decription of the experiments and discussion in the main text. Please be aware that the bubbles seen in the ponceau are in between the membrane and the glass support for the picture and not on the membrane. All cells were cultured photoautotrophically in HSM.

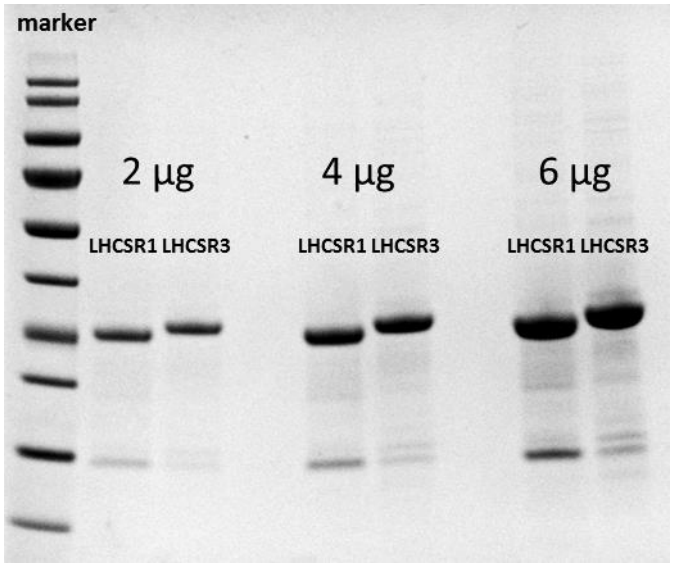

Fig. S3 . SDS-PAGE stained with Coomassie brilliant blue staining showing the purity of the LHCSRs inclusion bodies.

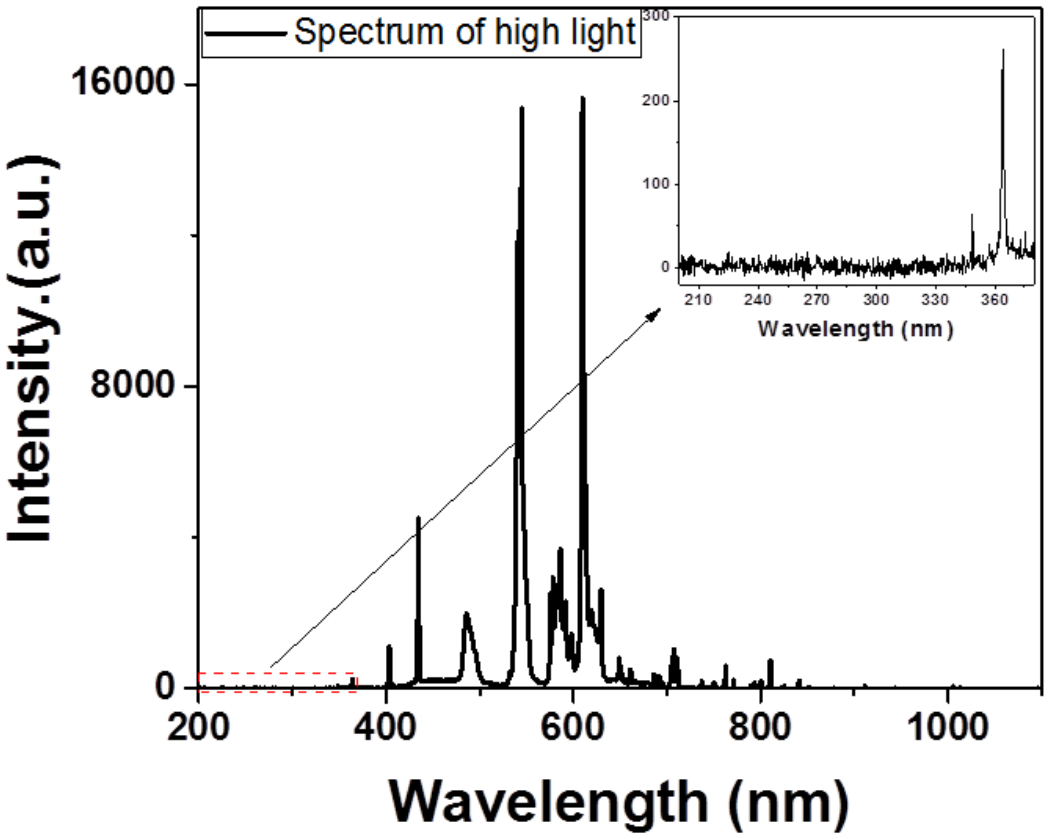

Fig. S4 the light spectrum of the light source used to grow the alga in this work. The inset shows the spectrum between 200 nm to 380 nm.

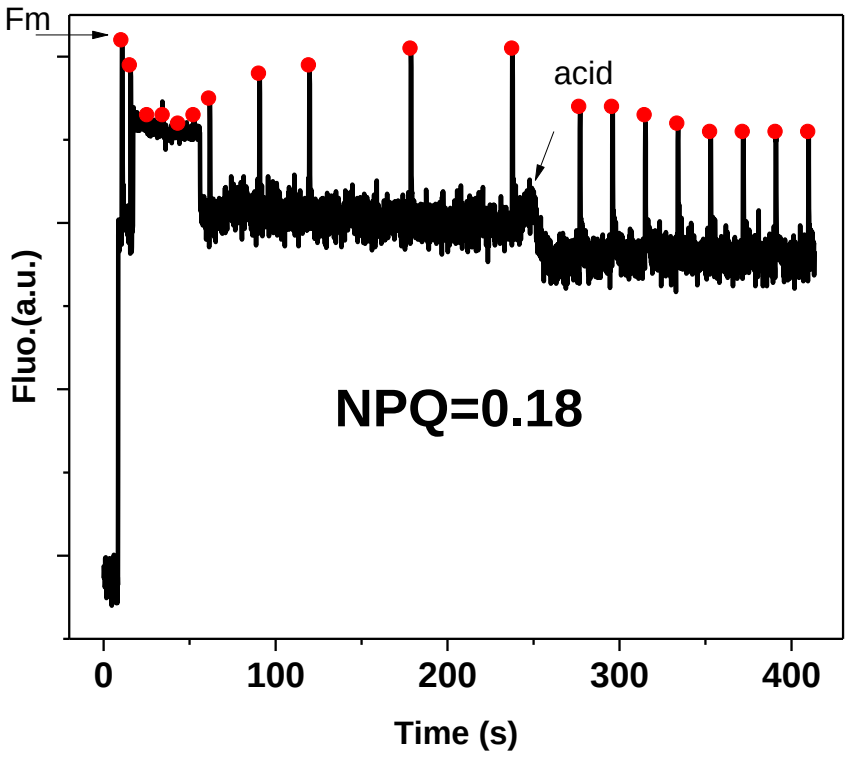

Fig.S5 The fluorescence trace for *npq4/stt7-9* double mutant that grown under high light in HSM. The onset of the initial light-induced NPQ is visible at t = 15 s, followed by the dark relaxation after t = 60 s. The acid-induced quenching is observed after acetic acid addition at t = 250. Note the small NPQ amplitude in both of these cases. of the initial light-induced NPQ is visible at t = 15 s, followed by the dark relaxation after t = 60 s. The acid-induced quenching is observed after 5 mM acetic acid addition at t = 250 s.

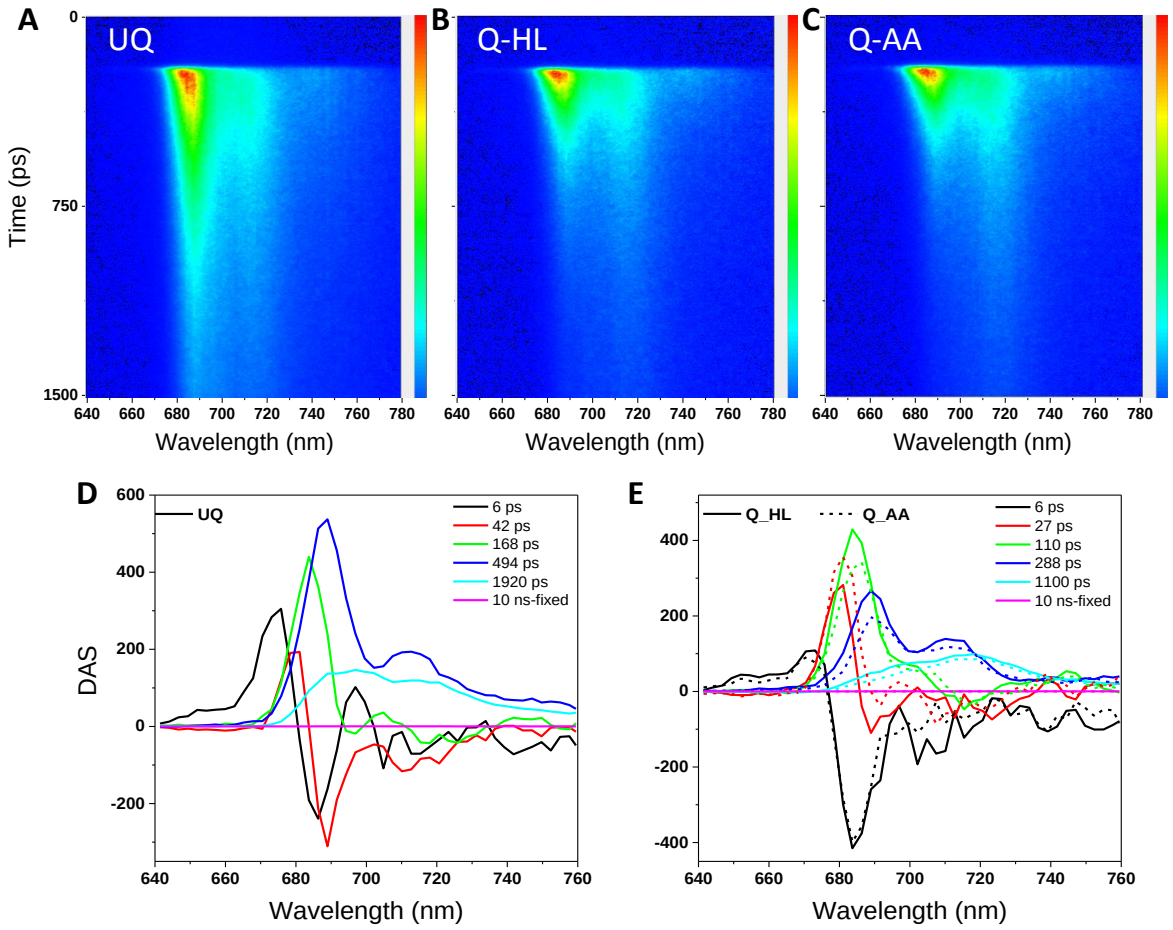

Fig. S6 Time-resolved fluorescence images and the fitting results at 77K. Streak camera images of intact cells in different fluorescence states: Unquenched—UQ (***A***), quenched by high light—Q-HL(***B***), and by acetic acid—Q-AA-pH 5.5 (***C***). Decay Associated Spectra (DAS) of unquenched cells (UQ) (***D***), DAS of quenched cells by HL (Q_HL,solid lines) and by acid (Q_acid, dashed lines) (***E***). The corresponding lifetimes are listed in the figure legend. For the spectra of 10 ns see Figure S2, and the assignment of the components to specific processes see table S1.

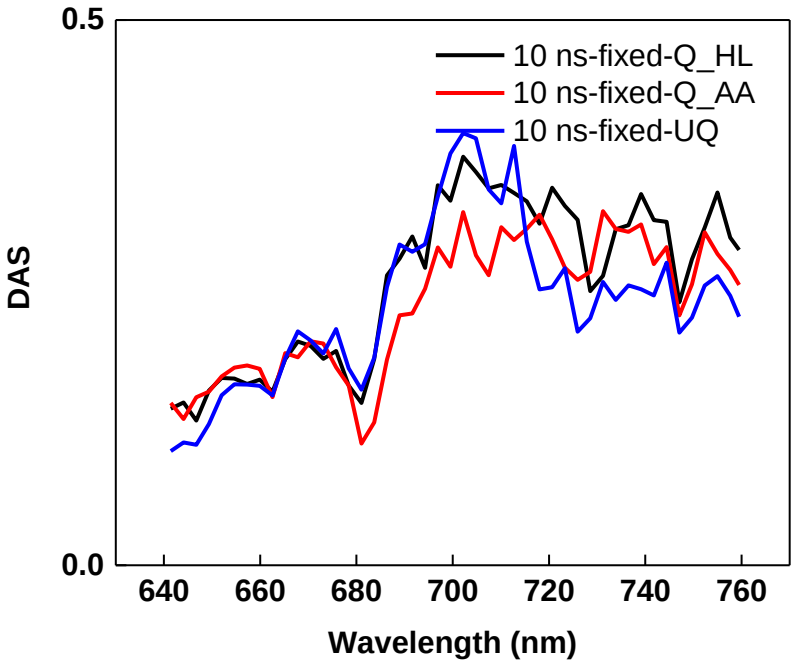

Fig.S7 The DAS of the 10 ns lifetime component at 77K (see Fig.S6 for details)

Table S1. Global analysis results of the time-resolved fluorescence of cells at 77K. *the assignments to different processes are made based on spectra and lifetimes. In addition, a longer component (lifetime fixed to 10 ns) probably due to some background noise with a contribution <0.1% was present (Fig.S6). The 6 ps component is within the instrument response function (IRF), therefore should be considered with caution. EET – Excitation Energy Transfer.

	UQ (ps)	Q (ps)	Assignments*
τ1	6	6	EET within LHCII trimer
τ2	38	27	EET within PSII/PSI
τ3	138	110	EET within PSII/PSI
τ4	317	288	Trapping in PSII/PSI after full equilibrium
τ5	1100	1100	Red traps in PSII/LHCI-PSI

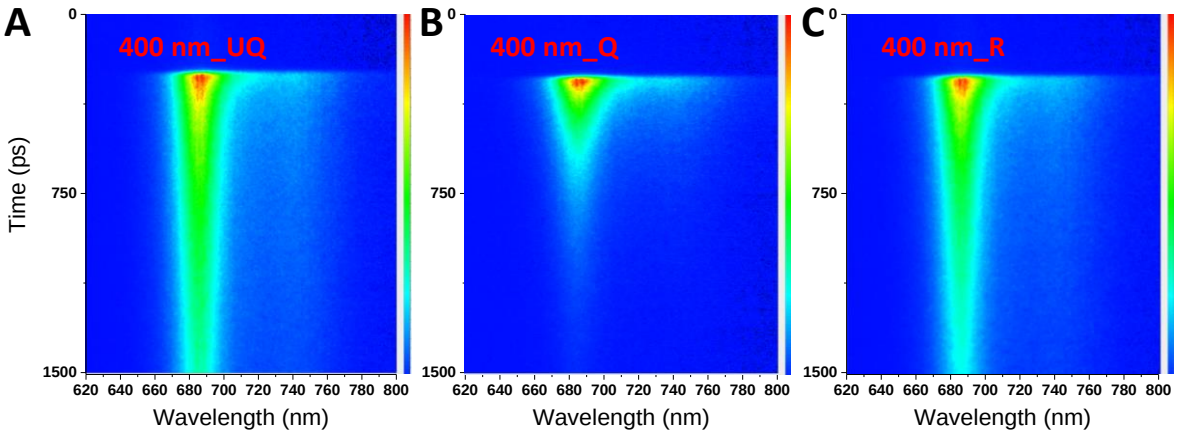

Fig.S8. Streak camera images of *C. reinhardtii* cells at RT in three fluorescence states. (***A***), unquenched (UQ), (***B***), quenched (Q) and (***C***), recovered (R) upon 400 nm excitation. Cells were kept in UQ, Q (with acid) and R (with KOH) states as illustrated in Fig. 1 of the main manuscript.

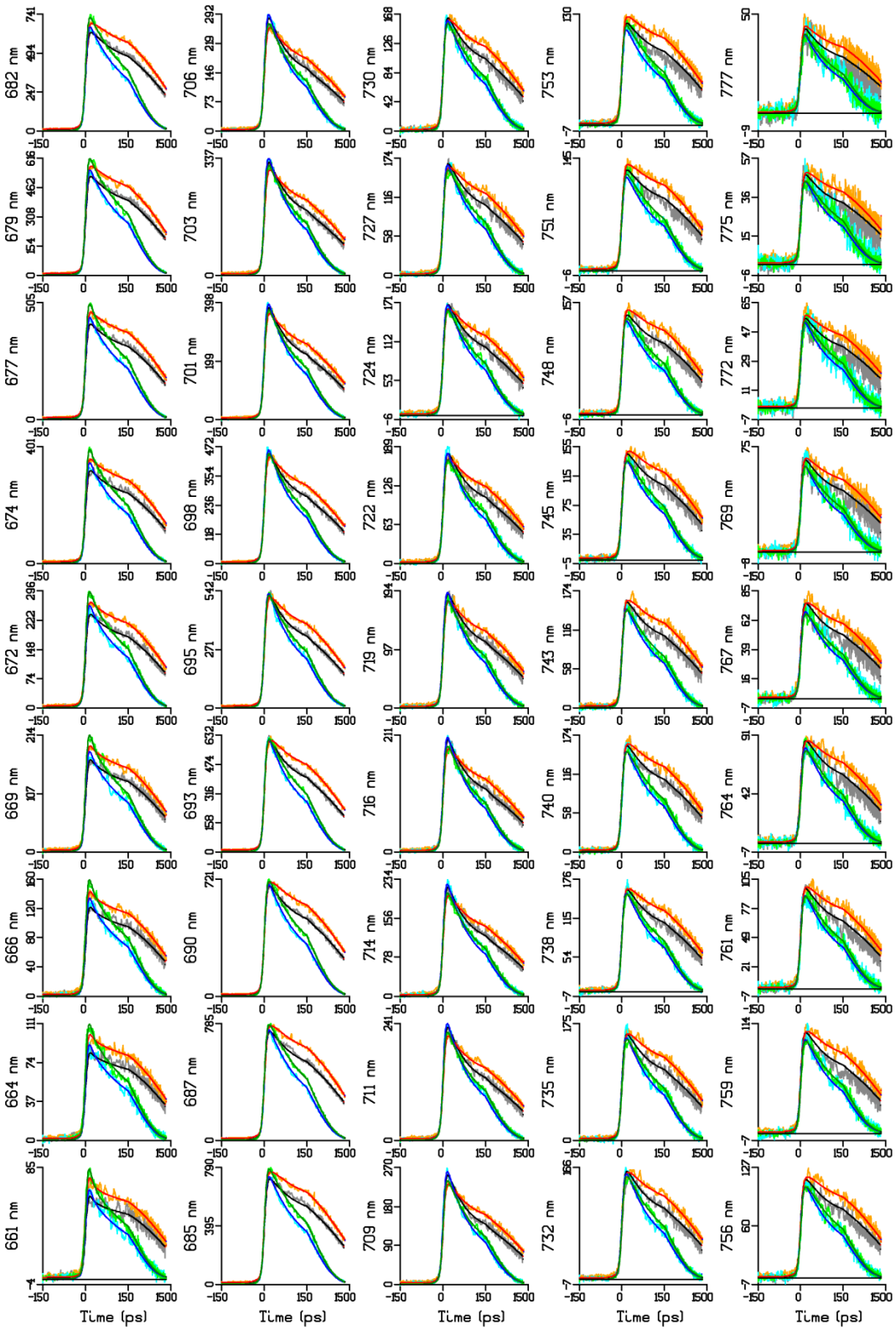

Fig. S9 Fluorescence decay curves of *C. reinhardtii* cells at RT and their fits at 45 wavelengths from four different experiments: unquenched _400 nm (black), unquenched _475 nm (red), quenched_400 nm (blue) and quenched_475 nm (green). The time axis is linear until 150 ps and logarithmic after that.

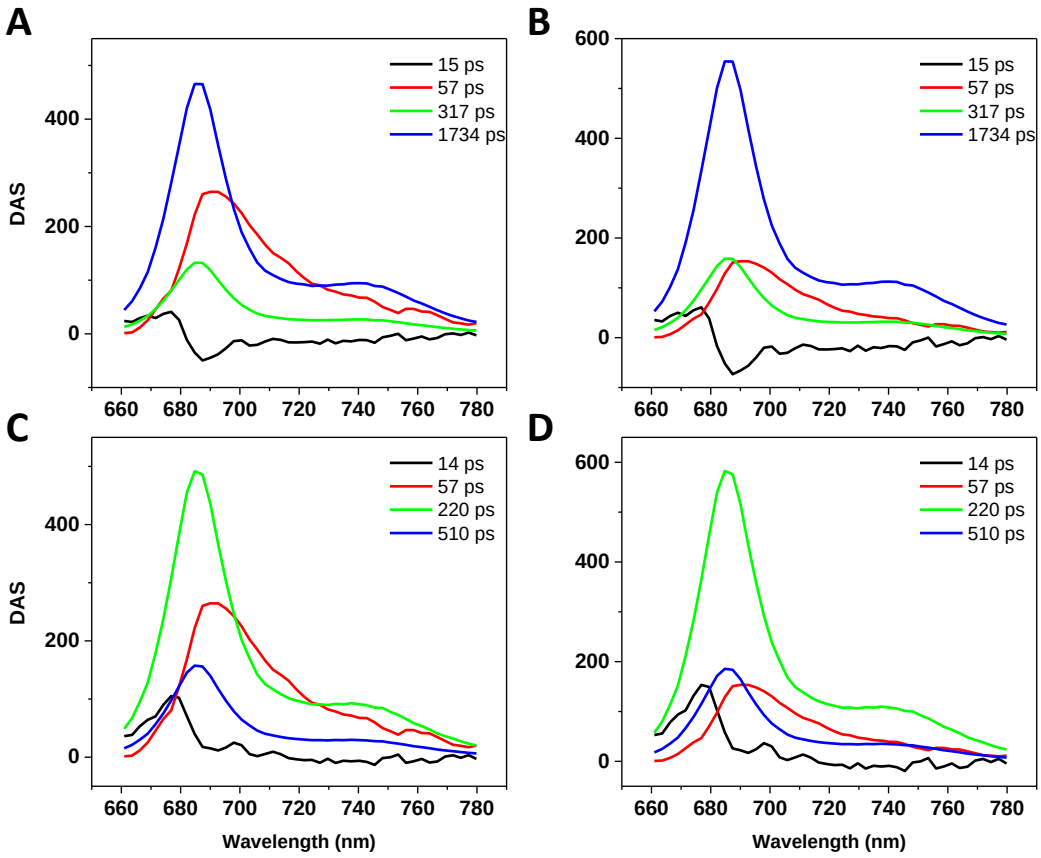

Fig. S10 Decay Associated Spectra (DAS) estimated from target analysis on unquenched (***A*** and ***B***) and quenched (***C*** and ***D***) *C. reinhardtii* cells upon excitations at 400 nm (***A*** and ***C***) and 475 nm (***B*** and ***D***) at RT. The Lifetimes are indicated in the Figures.

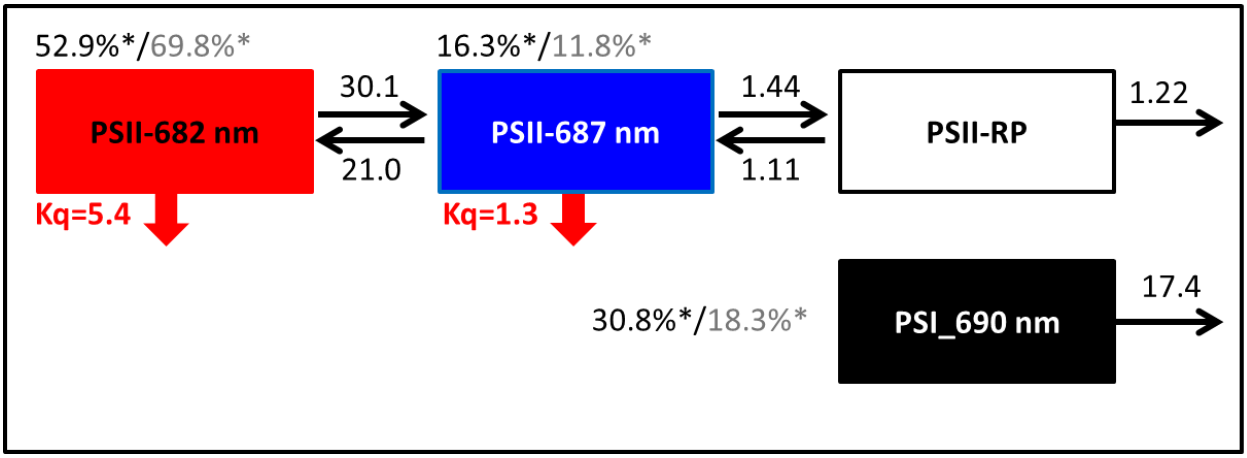

Fig. S11 An alternative model for the time-resolved fluorescence data at RT with additional quenching pathways, rates are given in $(ns)^{-1}$, Kqs are the rates of quenching, * indicates the initial excitation at 400 nm (black) and 475 nm (grey).

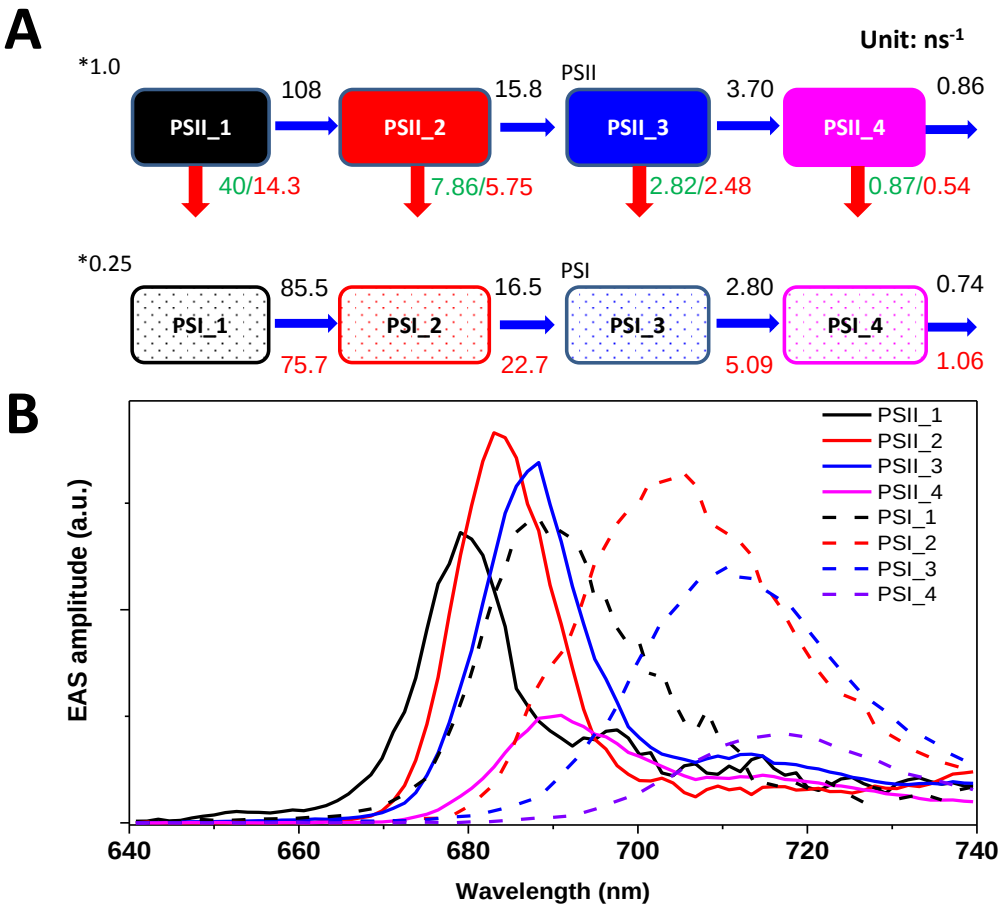

Fig. S12 Sequential target analysis of the *C. reinhardtii* cells at 77K. **(*A*),** Scheme of the sequential model used, PSI or PSII_1-4 represent the initial (1),intermediate (2&3) and final state (4) of PSI and PSII kinetics, respectively. **(*B*),** Evolution Associated Spectra (EASs) were estimated for each compartment. Initial excitations on PSII and PSI are given (*). All rate constants (in ns^{-1}) are treated as ''free-fitting'' parameters and indicated in the scheme, UQ_PSII (black only), Q_Acid_PSII (black and green), QHL_PSII (black andred), PSI in the cells (black) and isolated PSI (red).

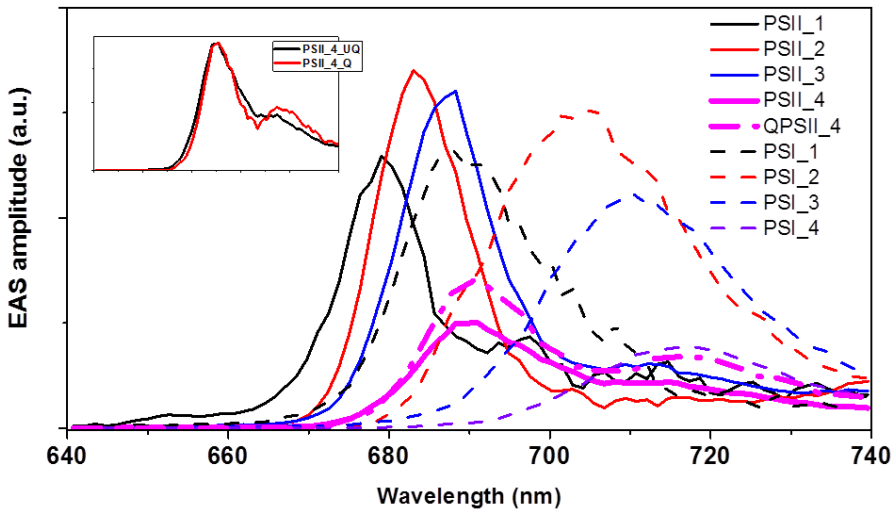

Fig. S13 Sequential target analysis of *C. reinhardtii* cells at 77K. For this analysis the same scheme shown in Figure S12 was used, but the spectra of QPSII_4 and UQPSII_4 we unlinked. The resulting spectra of PSII_4_UQ and PSII_4_Q normalized to maxmium are shown in the inset.

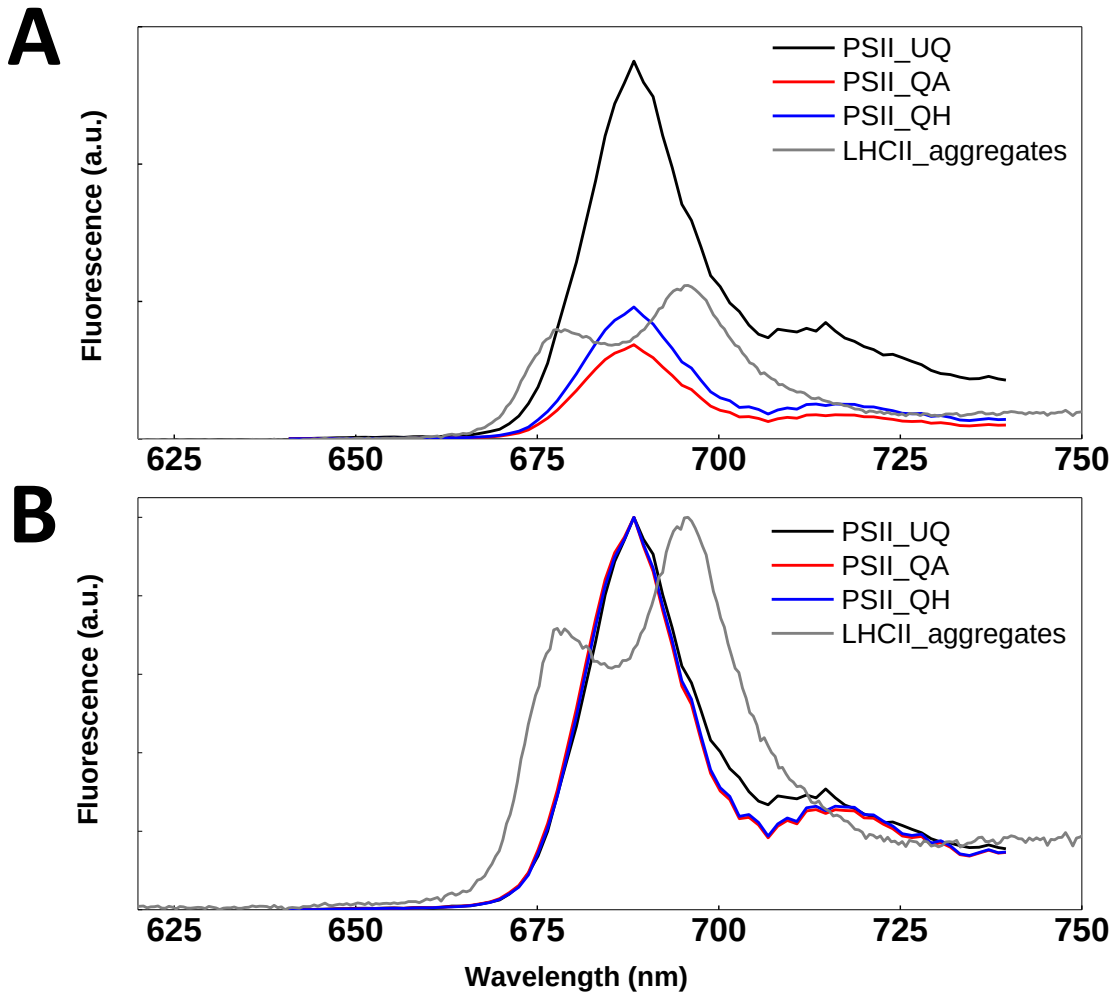

Fig. S14 Comparison of the reconstructed steady-state PSII fluorescence spectra with the spectrum of LHCII-aggregates at 77K (9). (***A***),PSII and LHCII-aggregates emission spectra. (***B***),The spectra are normalized to the maximum. The PSII spectra of UQ (PSII_UQ), Q_Acid (PSII_QA) and Q_HL (PSII_QH) were reconstructed from their target analysis models in Fig. S12.

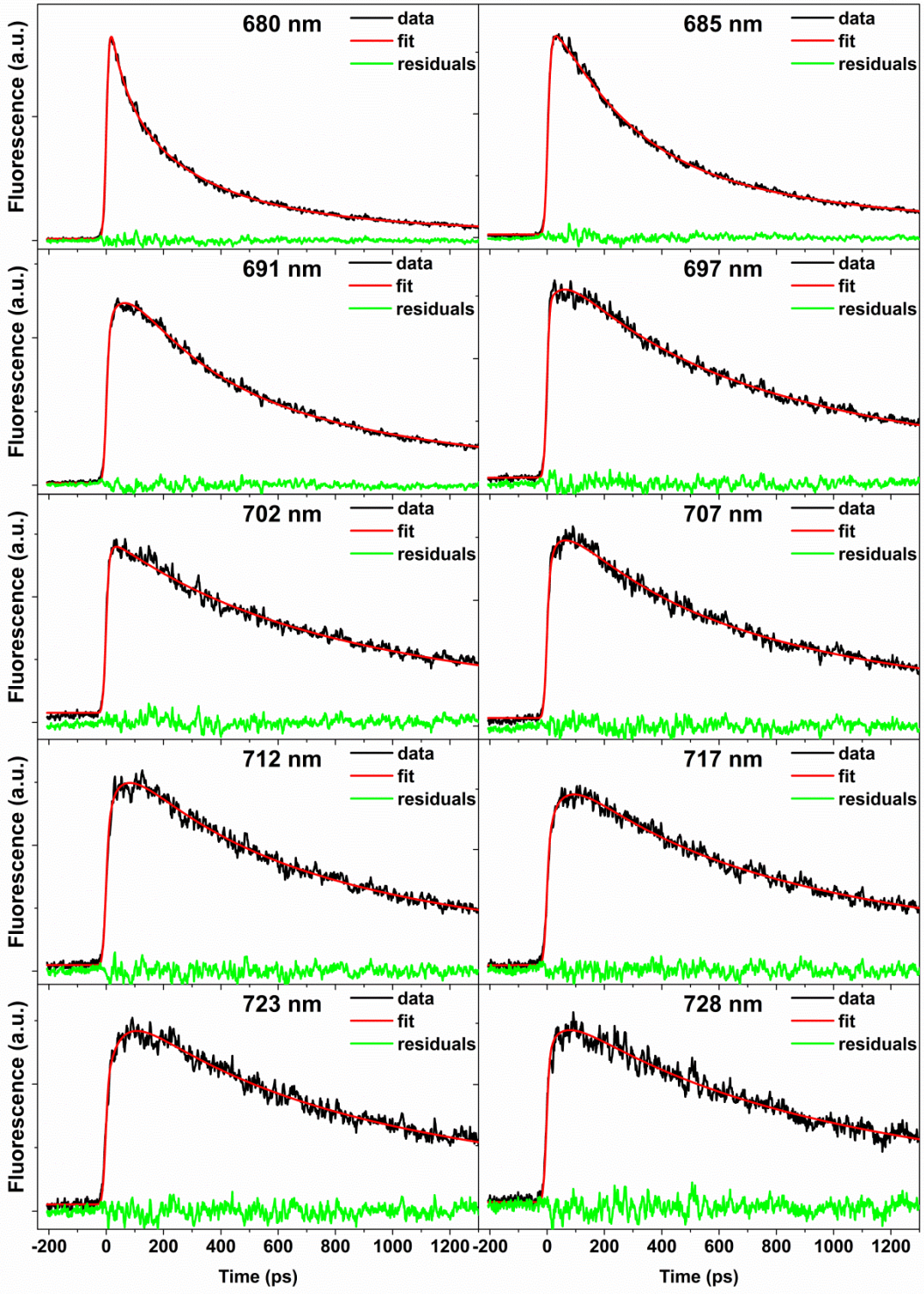

Fig. S15 Time-traces of unquenched *C. reinhardtii* cells upon 475 nm excitation at 77K and their fitted curves.

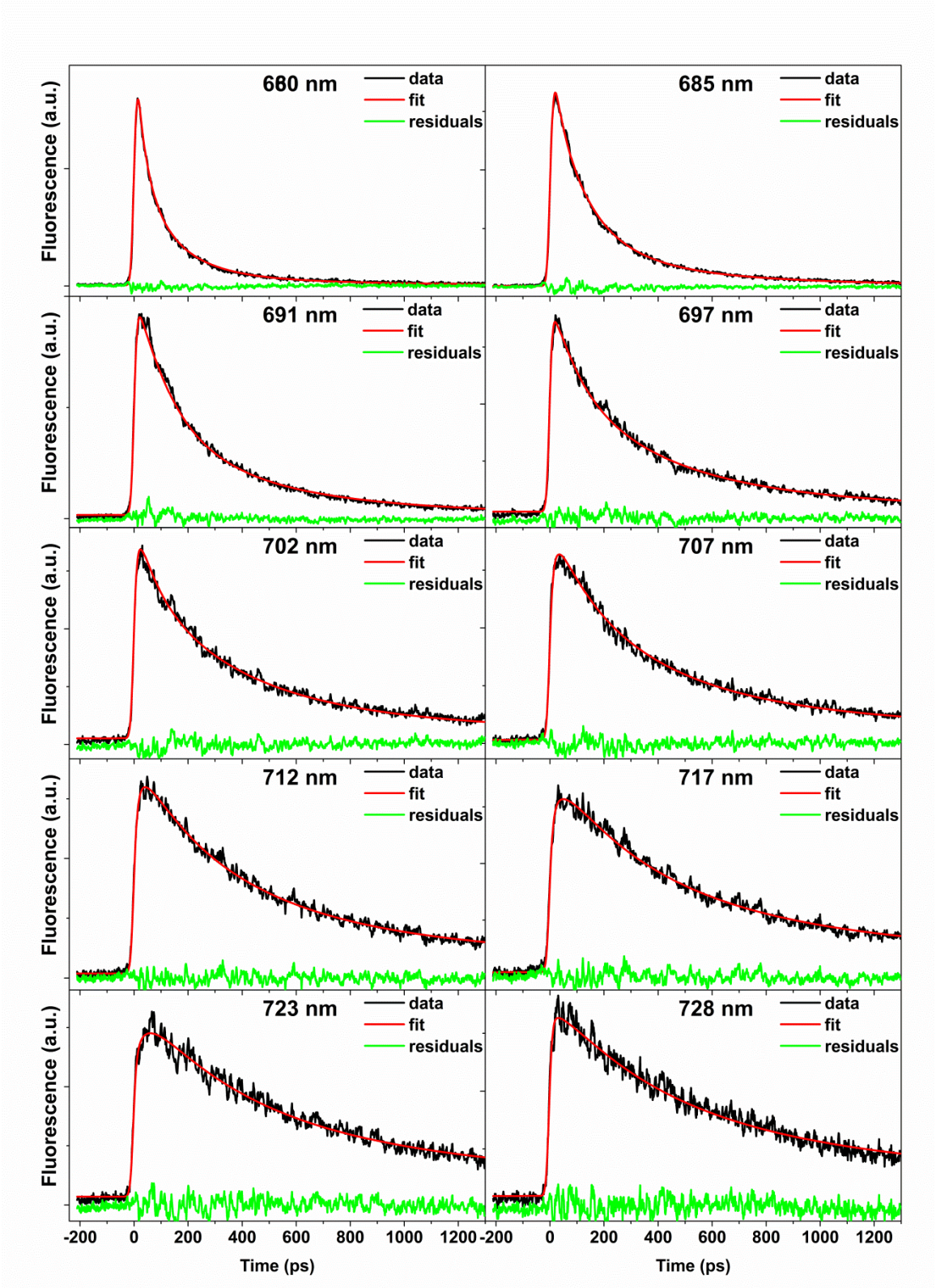

Fig.S16 Time-traces of acetic acid-induced quenched *C. reinhardtii* cells upon 475 nm excitation at 77K and their fitted curves.

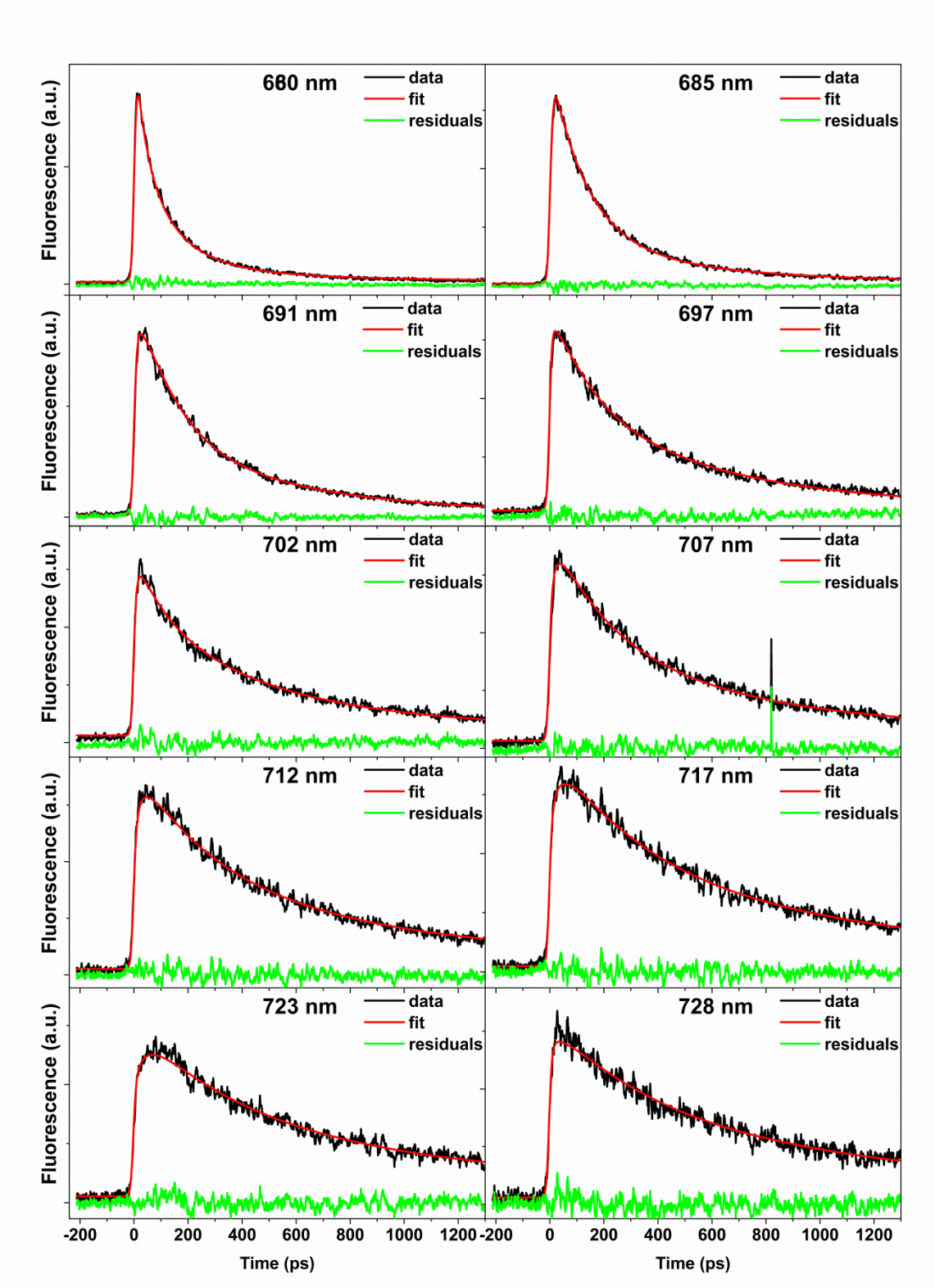

Fig.S17 Time-traces of high light-induced quenched *C. reinhardtii* cells upon 475 nm excitation at 77K and their fitted curves.

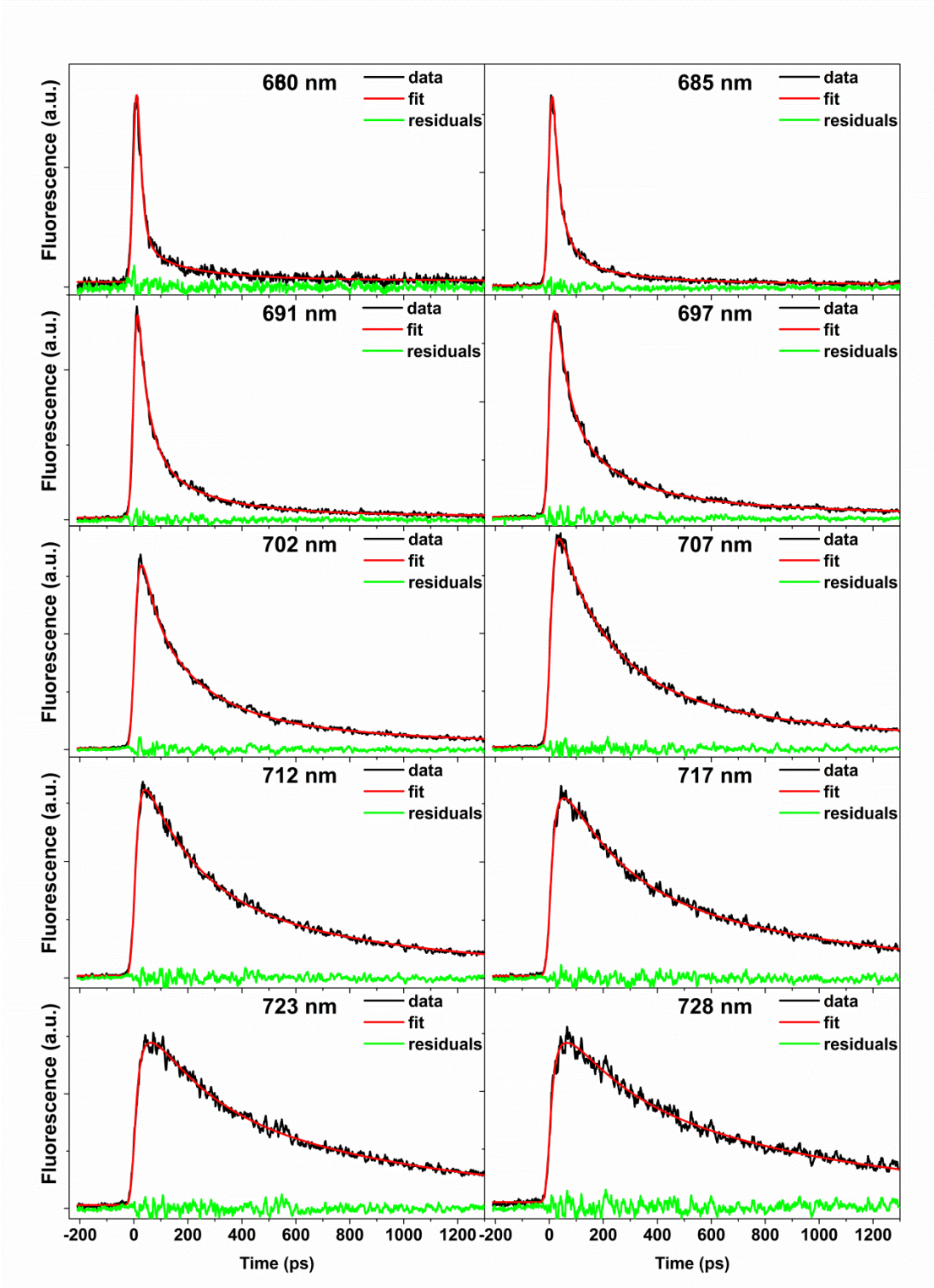

Fig. S18 Time-traces of isolated Photosystem I complex upon 400 nm excitation at 77K and their fitted curves.

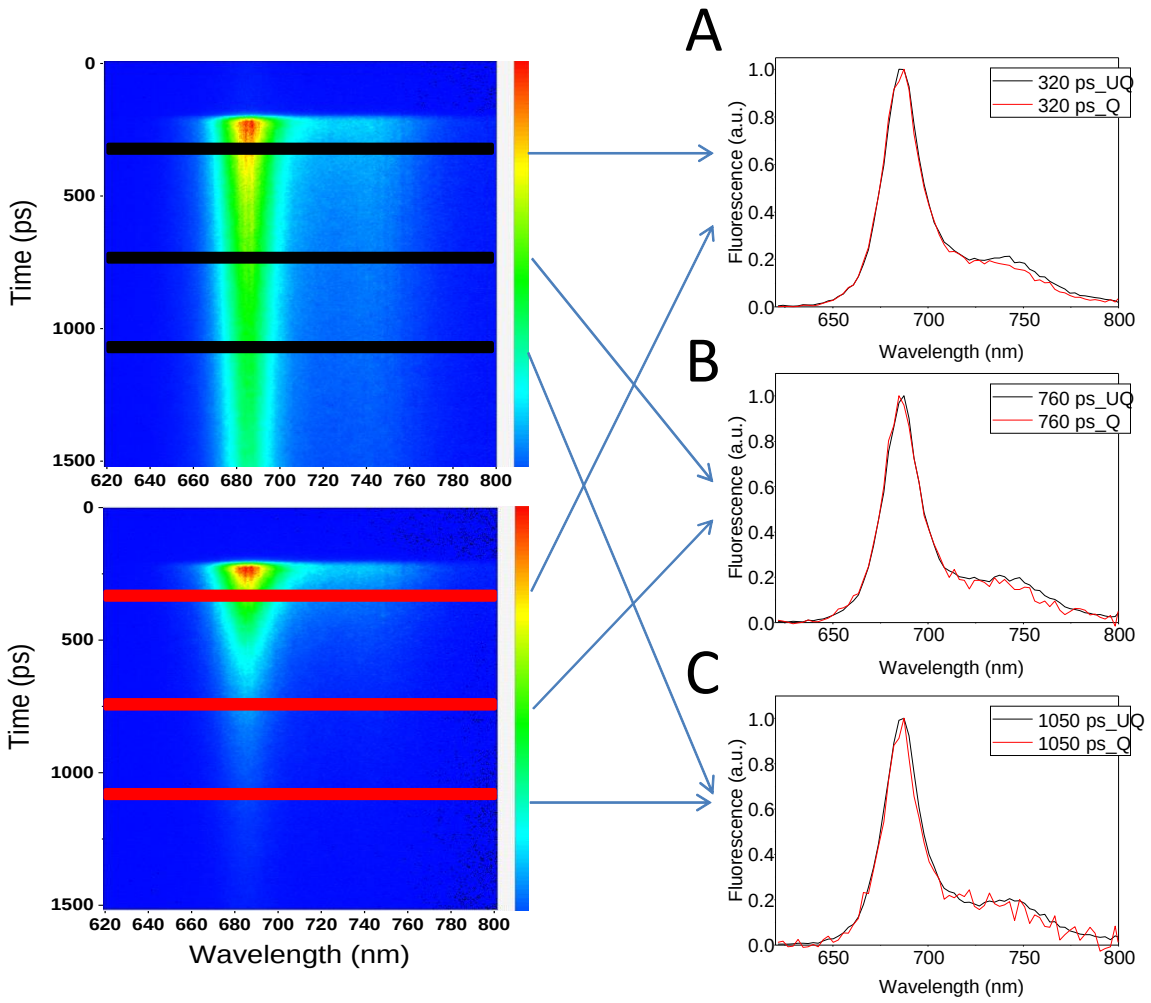

Fig. S19 Normalized emission spectra at RT of UQ and Q cells taken from the streak images (left panel, same as in Fig. 2 ***A*** and ***B*** at different time points after excitation: **(*A*)**, t=320 ps; (***B***), t=760 ps and (***C*****),** t=1050 ps.

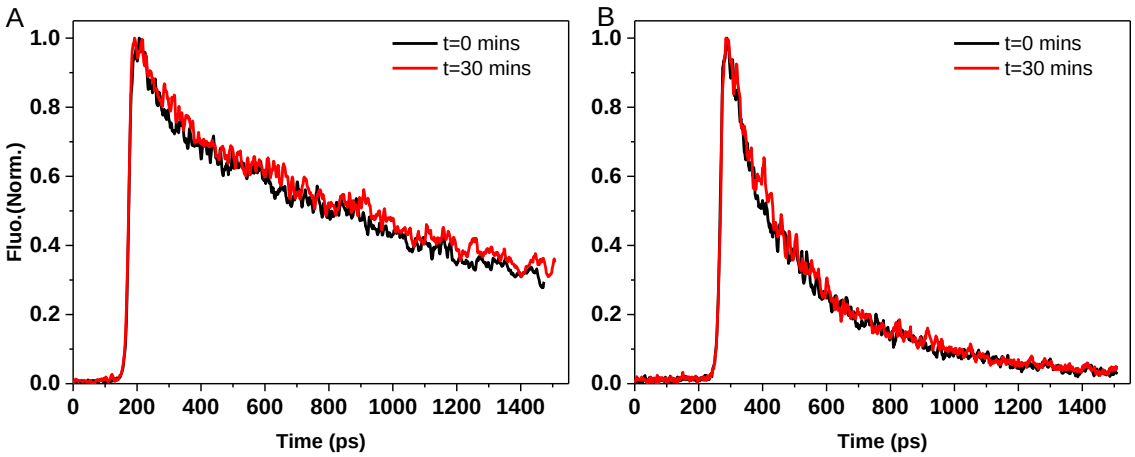

Fig. S20 Normalized fluorescence dacay traces at RT at 680 ±5 nm of UQ (***A***) and Q (***B***) cells. Excitation wavelength was 400 nm, t represents the approximate time when a set of 10 images (averaged) in one sequence of 200 was collected.

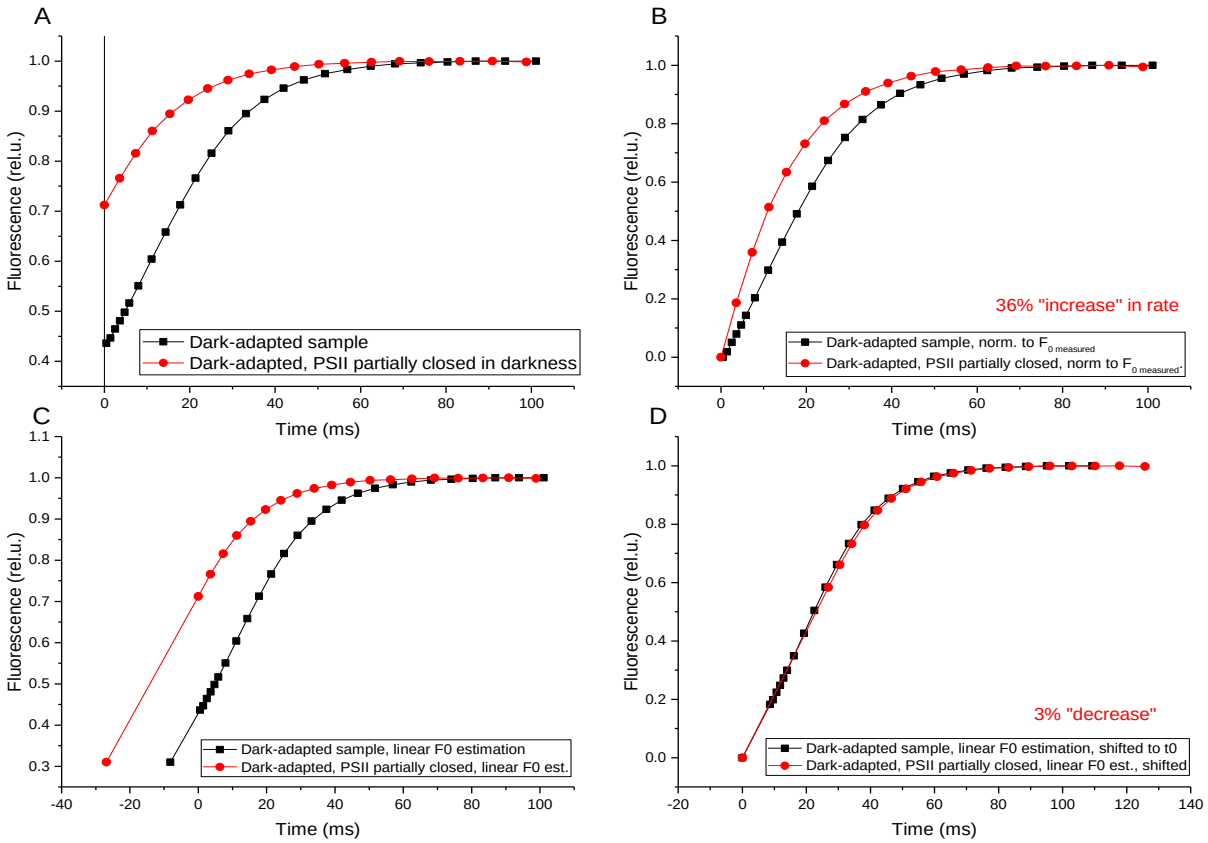

Fig. S21 Determination of the functional PSII antenna size in quenched state. The Fig. shows the importance of taking into account the presence of closed RCs to the estimation of the functional antenna size of PSII with the fluorescence induction curve in DCMU. RCs can be closed by light, but also due to non-photochemical reduction of the PQ pool, in equilibrium with Q_A ; the addition of DCMU always results in a closure of some RCs (see text and supp.text 3). (*A*) traces of fluorescence induction in a dark-adapted sample (black), and the same kinetics but when part of the PSII RCs were closed (red); (*B*) the traces from panel A, normalized between 0 and 1. A comparison of the areas above the fluorescence curve indicates that the antenna size of the sample with partially closed PSII RCs is 36% larger. This result is an artifact due to the assumption that the initial level of fluorescence, $F_{0\ measured}$, is recorded when with all the centres open; and the apparent increase is due to the contribution of closed PSII to the photochemical rate of the open RCs during illumination. (*C*) Linear extrapolation to the initial F_0. Initial points from both curves were used for a linear fitting to find the x-axis value of the dark-adapted F_0 value in the absence of DCMU. (*D*) The curves from panel C after translation of the x axis to 0 for each F_0 timepoint. One notices that the areas above those curves are almost identical, therefore the compensation for initially closed PSII was successful.

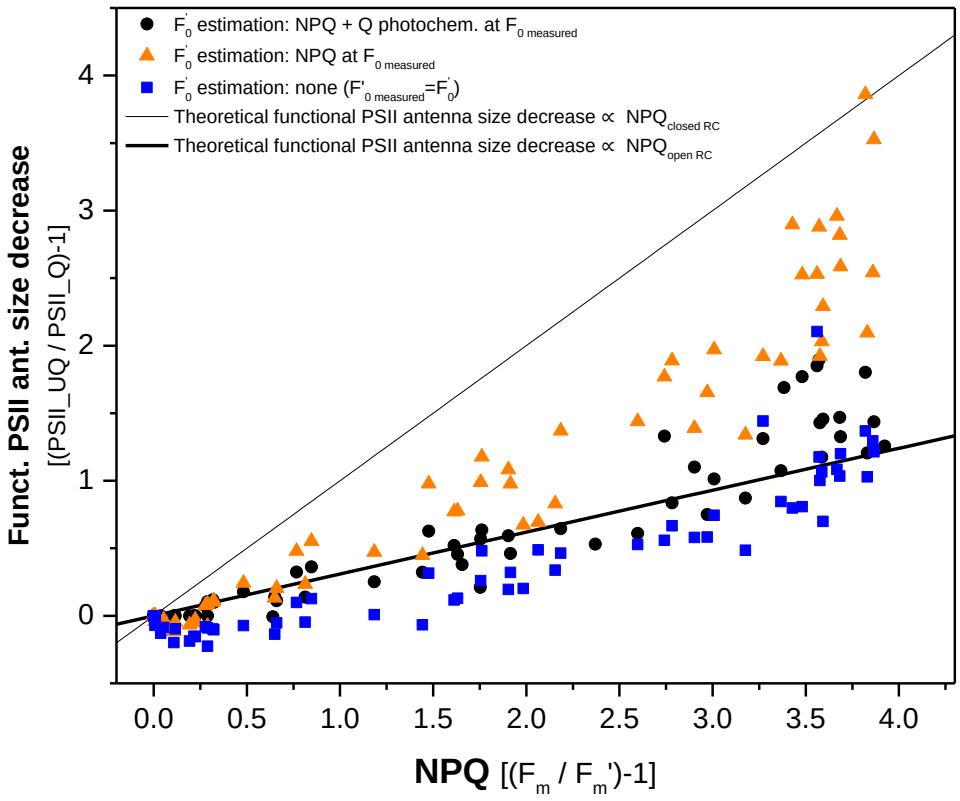

Fig. S22 Decrease of the functional antenna size of PSII as a function of NPQ for three modes of F_0' estimation. See supp. Text 3 for details. Similarly to the Fig. 4, the black circles show the situation where F_0' was estimated assuming an identical NPQ rate for closed- and open RCs but taking into account the presence of photochemical quenching in the latter case. Orange triangles show the estimation where F_0 is quenched to the same extent as F_M, i.e. both 50% in the case of NPQ 1 (F_V/F_M unchanged upon quenching). Blue squares show the situation for no F_0' estimation (i.e. assumption that $F'_{0\ measured} = F'_{0\ actual}$). This is because after actinic illumination the electron transfer chain becomes reduced, and the addition of DCMU results in a large fraction of RCs becoming closed – due to a large amount of PSII in $QB^{\cdot-}$ state which is present shortly after illumination (11).

References

1. Chua NH, Bennoun P (1975) Thylakoid Membrane Polypeptides of Chlamydomonas-Reinhardtii - Wild-Type and Mutant Strains Deficient in Photosystem 2 Reaction Center. *Proc Natl Acad Sci USA* 72(6):2175-2179.
2. Dinc E, et al. (2016) LHCSR1 induces a fast and reversible pH-dependent fluorescence quenching in LHCII in Chlamydomonas reinhardtii cells. *Proc Natl Acad Sci U S A* 113(27):7673-7678.
3. Croce R, Canino G, Ros F, Bassi R (2002) Chromophore Organization in the Higher-Plant Photosystem II Antenna Protein CP26. *Biochem* 41(23):7334-7343.
4. Correa-Galvis V, et al. (2016) Photosystem II Subunit PsbS Is Involved in the Induction of LHCSR Protein-dependent Energy Dissipation in Chlamydomonas reinhardtii. *Journal of Biological Chemistry* 291(33):17478-17487.
5. Tibiletti T, Auroy P, Peltier G, Caffarri S (2016) Chlamydomonas reinhardtii PsbS Protein Is Functional and Accumulates Rapidly and Transiently under High Light. *Plant physiology* 171(4):2717-2730.
6. Allorent G, et al. (2016) UV-B photoreceptor-mediated protection of the photosynthetic machinery in Chlamydomonas reinhardtii. *Proceedings of the National Academy of Sciences of the United States of America* 113(51):14864-14869.
7. van Stokkum IH, Larsen DS, van Grondelle R (2004) Global and target analysis of time-resolved spectra. *Biochim Biophys Acta* 1657(2-3):82-104.
8. Miloslavina Y, et al. (2008) Far-red fluorescence: a direct spectroscopic marker for LHCII oligomer formation in non-photochemical quenching. *Febs Lett* 582(25-26):3625-3631.
9. Natali A, et al. (2016) Light-harvesting complexes (LHCs) cluster spontaneously in membrane environment leading to shortening of their excited state lifetimes. *J Biol Chem* 291(32):16730-16739.
10. Sueoka N (1960) Mitotic replication of deoxyribonucleic acid in Chlamydomonas reinhardi. *Proc Natl Acad Sci U S A* 46(1):83-91.
11. Lazár D (1999) Chlorophyll a fluorescence induction. *Biochim Biophys Acta* 1412(1):1-28.
12. Lavorel J, Joliot P (1972) A connected model of the photosynthetic unit. *Biophys J* 12(7):815-831.
13. Belgio E, et al. (2014) Economic photoprotection in photosystem II that retains a complete light-harvesting system with slow energy traps. *Nat Commun* 5:4433.
14. Magyar M, et al. (2018) Rate-limiting steps in the dark-to-light transition of Photosystem II - revealed by chlorophyll-a fluorescence induction. *Scientific Reports* 8.
15. Schansker G, Toth SZ, Kovacs L, Holzwarth AR, Garab G (2011) Evidence for a fluorescence yield change driven by a light-induced conformational change within photosystem II during the fast chlorophyll a fluorescence rise. *Biochimica Et Biophysica Acta-Bioenergetics* 1807(9):1032-1043.
16. Vredenberg WJ (2008) Analysis of initial chlorophyll fluorescence induction kinetics in chloroplasts in terms of rate constants of donor side quenching release and electron trapping in photosystem II. *Photosynthesis Research* 96(1):83-97.
17. Strasser RJ, Tsimilli-Michael M, Srivastava A (2004) Analysis of the Chlorophyll a Fluorescence Transient. *Chlorophyll a Fluorescence: A Signature of Photosynthesis*, eds Papageorgiou GCGovindjee (Springer Netherlands, Dordrecht), pp 321-362.
18. Endo T, Asada K (1996) Dark induction of the non-photochemical quenching of chlorophyll fluorescence by acetate in Chlamydomonas reinhardtii. *Plant Cell Physiol.* 37(4):551-555.
19. Farooq S, et al. (2018) Dynamic feedback of the photosystem II reaction centre on photoprotection in plants. *Nat Plants* 4(4):225-231.
20. Unlu C, Drop B, Croce R, van Amerongen H (2014) State transitions in Chlamydomonas reinhardtii strongly modulate the functional size of photosystem II but not of photosystem I. *Proc Natl Acad Sci U S A* 111(9):3460-3465.